Excited-State Geometry Optimization of Small Molecules with Many-Body Green's Functions Theory

Onur Çaylak* and Björn Baumeier*

Read Online

ACCESS | Metrics & More | Article Recommendations | SI Supporting Information

ABSTRACT: We present a benchmark study of gas phase geometry optimizations in the excited states of carbon monoxide, acetone, acrolein, and methylenecyclopropene using many-body Green's functions theory within the GW approximation and the Bethe−Salpeter equation (BSE) employing numerical gradients. We scrutinize the influence of several typical approximations in the GW-BSE framework; we used one-shot G_0W_0 or eigenvalue self-consistent evGW, employing a fully analytic approach or plasmon-pole model for the frequency dependence of the electron self-energy, or performing the BSE step within the Tamm−Dancoff approximation. The obtained geometries are compared to reference results from multireference perturbation theory (CASPT2), variational Monte Carlo (VMC) method, second-order approximate coupled cluster (CC2) method, and time-dependent density-functional theory (TDDFT). We find overall a good agreement of the structural parameters optimized with the GW-BSE calculations with CASPT2, with an average relative error of around 1% for the G_0W_0 and 1.5% for the evGW variants based on a PBE0 ground state, respectively, while the other approximations have negligible influence. The relative errors are also smaller than those for CC2 and TDDFT with different functionals and only larger than VMC, indicating that the GW-BSE method does not only yield excitation energies but also geometries in good agreement with established higher-order wave function methods.
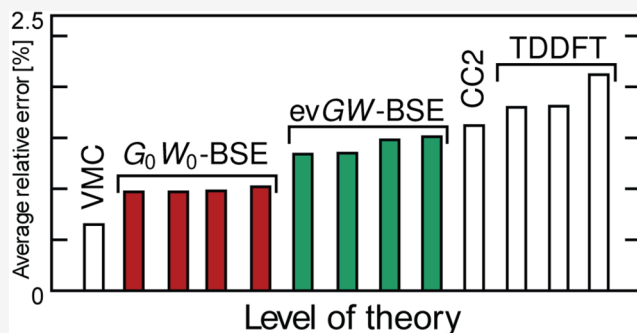
1. INTRODUCTION

Electronically excited molecules play a pivotal role in a wide range of processes and applications, for example, from photosynthesis to light-conversion processes in organic optoelectronic devices,[1−3] as probes in fluorescent spectroscopy,[4] or as intermediates in catalytic reactions.[5] From a computational perspective, excited-state properties are conventionally studied using either post-Hartree−Fock methods, such as a different version of configuration interaction or coupled cluster (CC) approaches, or time-dependent formulations of density-functional theory (TDDFT). However, the accuracy of these methods can sensitively depend on both the type of excitations (e.g., local vs charge-transfer type) studied and the details of the level of theory used, such as order of allowed excitations in CC or the functional in TDDFT.[6]

Inspired by its successes in the solid-state community, the use of many-body Green's functions theory[7−10] in the GW approximation with the Bethe−Salpeter equation (BSE) has attracted increasing attention for the calculation of electronic excitation in molecular systems in past years..[11−22] Starting from an N-electron (DFT) ground state, quasiparticle excitations for the removal and addition of an electron are calculated first in the GW step. Subsequently, the BSE is used to describe neutral excitations as coupled electron−hole pairs based on quasiparticle product functions.[9,23] This formulation is similar to linear-response TDDFT in the Casida formulation[24] with comparable computational cost and can be used to predict excitation energies for different types of excitations with good accuracy.[13,14]

Focuses of the studies based on GW-BSE have nearly exclusively focused on excitation energies based on ground-state geometries, i.e., absorption energies. Only a few efforts have been directed at investigations of geometric relaxations after excitation and/or emission energies. The total energy of the excited state S depending on nuclear coordinates $\boldsymbol{R}$ is given as $E_S(\boldsymbol{R}) = E_0(\boldsymbol{R}) + \Omega_S(\boldsymbol{R})$, where E_0 is the ground-state energy and Ω_S the excitation energy. Taking its gradient with respect to the nuclear coordinates, $\partial_{\boldsymbol{R}} E_S$, shows that it is a sum of the standard gradient of the ground-state energy and the gradient of the excitation energy, $\partial_{\boldsymbol{R}}\Omega_S$. Ismali-Beigel and Louie[25] discussed that by employing the Hellman−Feynman theorem the latter contribution can be evaluated as

$$\partial_{\boldsymbol{R}}\Omega_S = \langle S|\partial_{\boldsymbol{R}}\hat{H}^{BSE}|S\rangle \tag{1}$$

where $\hat{H}^{\mathrm{BSE}}$ is the two-particle Hamiltonian of the BSE for the electron−hole pair (see Section 2). This Hamiltonian contains the contributions from the single quasiparticles as given by the GW approximation and their interactions. The central quantity in GW-BSE is the nonlocal, energy-dependent electron self-energy operator,[26] which contains many-body effects, or electron correlation. It is given as the convolution in the frequency domain of the one-electron Green's function G and a screened Coulomb interaction W typically evaluated using the random-phase approximation (RPA). Due to its form, no exact analytic expressions are available for the evaluation of eq 1, and one has in practice to rely on numerical gradients instead. This complication is further exacerbated by the fact that different approaches can be used both on the GW and BSE levels: the GW convolution can be performed with exact fully analytic (FAA) methods[10,18,22] or simplifications, such as a plasmon-pole model[26] (PPM). The self-energy operator also implicitly depends on the quasiparticle energies $\varepsilon_i^{\mathrm{QP}}$ via G and W. In the G_0W_0 approach, both quantities are constructed using the Kohn−Sham (KS) single-particle energies $\varepsilon_i^{\mathrm{KS}}$ of the underlying DFT calculation. Furthermore, the obtained $\varepsilon_i^{\mathrm{QP}}$ can be used in the construction of an updated self-energy operator, followed by the determination of improved quasiparticle energies. This procedure can either be repeated n times (G_nW_n) or until self-consistency in the energies is reached (evGW). On top of this, the BSE can either be used in its full form including resonant−antiresonant coupling terms or within the Tamm−Dancoff approximation (TDA). Benchmarking excitation energies[16,21,27] has revealed that best accuracy with respect to the theoretical best estimate is achieved with the evGW-BSE/full/FAA variant, with the underlying DFT ground-state calculation performed with a hybrid functional, typically PBE0.[28] A systematic analysis of the accuracy of excited-state geometries using GW-BSE, in general, and the influence of the specific methodological choices mentioned above intrinsic to the GW-BSE steps, in particular, has not been performed, to date.

Here, we give a benchmark of optimized excited-state geometries for a set of standard small molecules comprising carbon monoxide, acetone, s-cis and s-trans acrolein, and methylenecyclopropene (MCP) in different symmetries and covering both $n \rightarrow \pi^*$ and $\pi \rightarrow \pi^*$ excitations.[29−31] We briefly discuss the suitability of the various quasiparticle self-consistency choices in the GW step for the calculation of numerical gradients by inspection of the one-dimensional excited-state potential energy surface (PES) of CO and also highlight the influence of the different self-energy models and the BSE types. Then, we focus on eight variants of the GW-BSE approach for the rest of the molecular set and evaluate them against each other. The obtained geometries are compared to reference data from the methods CASPT2, variational Monte Carlo (VMC), CC2, and TDDFT with the PBE0,[28] CAM-B3LYP,[32] and M06-2X[33] functionals, respectively, in order to assess how reliable GW-BSE-based excited-state geometries are.

This article is organized as follows: In Section 2, we briefly summarize the essential theoretical and computational details of GW-BSE. In Section 3, we show and discuss the results for the excited-state geometry optimizations of the small molecule set as obtained by the different variations of the GW-BSE calculations. A brief summary concludes the paper.

2. METHODOLOGY

2.1. Theoretical Framework. The molecules studied in this work exhibit a spin-singlet, closed-shell ground state with N

electrons. Within DFT, it is obtained by solving the Kohn−Sham equations[34]

$$\hat{H}^{\mathrm{KS}}|\phi_i^{\mathrm{KS}}\rangle = [\hat{H}_0 + \hat{V}_{\mathrm{xc}}]|\phi_i^{\mathrm{KS}}\rangle = \varepsilon_i^{\mathrm{KS}}|\phi_i^{\mathrm{KS}}\rangle \tag{2}$$

where $\hat{H}_0 = \hat{T}_0 + \hat{V}_{\mathrm{ext}} + \hat{V}_{\mathrm{H}}$, with $\hat{T}_0$ being the kinetic energy, $\hat{V}_{\mathrm{ext}}$ an external potential, $\hat{V}_{\mathrm{H}}$ the Hartree potential, and $\hat{V}_{\mathrm{xc}}$ the exchange-correlation potential.

The addition ($N \rightarrow N + 1$) or removal ($N \rightarrow N - 1$) of a single electron to/from the system can be treated as the excitation of a quasiparticle (QP). The QP states obey a Dyson-type equation of motion[11,35]

$$[\hat{H}_0 + \hat{\Sigma}(\varepsilon_i^{\mathrm{QP}})]|\phi_i^{\mathrm{QP}}\rangle = \varepsilon_i^{\mathrm{QP}}|\phi_i^{\mathrm{QP}}\rangle \tag{3}$$

where $\varepsilon_i^{\mathrm{QP}}$ are the one-particle excitation energies of the system, and $|\phi_i^{\mathrm{QP}}\rangle$ are the QP wave functions. Exchange-correlation effects are included via the electron self-energy operator $\hat{\Sigma}(E)$, which is expressed in the GW approximation as a convolution of the one-particle Green's function with the screened Coulomb interaction $W = \epsilon^{-1}v_c$, where $v_c(\mathbf{r}, \mathbf{r}') = |\mathbf{r} - \mathbf{r}'|^{-1}$ is the bare Coulomb interaction and $\epsilon^{-1}(\mathbf{r}, \mathbf{r}', \omega)$ is the inverse dielectric function calculated in the random-phase approximation (RPA).[8] Explicitly it reads

$$\Sigma(\mathbf{r}, \mathbf{r}', \omega) = \frac{\mathrm{i}}{2\pi}\int d\omega' G(\mathbf{r}, \mathbf{r}', \omega + \omega')W(\mathbf{r}, \mathbf{r}', \omega) \tag{4}$$

In practice, a basis of KS states is used to express the QP wave functions, i.e., $|\phi_i^{\mathrm{QP}}\rangle = \sum_j a_j^i |\phi_j^{\mathrm{KS}}\rangle$, which turns eq 3 into

$$H_{ij}^{\mathrm{QP}}(E) = \varepsilon_i^{\mathrm{KS}}\delta_{ij} + \langle\phi_i^{\mathrm{KS}}|\hat{\Sigma}(E) - \hat{V}_{\mathrm{xc}}|\phi_j^{\mathrm{KS}}\rangle \tag{5}$$

If the off-diagonal elements are small, the diagonal elements H_{ii}^{QP} are the sought quasiparticle energies and can be evaluated perturbatively according to

$$\varepsilon_i^{\mathrm{QP}} = \varepsilon_i^{\mathrm{KS}} + \Delta\varepsilon_i^{GW} = \varepsilon_i^{\mathrm{KS}} + \langle\phi_i^{\mathrm{KS}}|\hat{\Sigma}(\varepsilon_i^{\mathrm{QP}}) - \hat{V}_{\mathrm{xc}}|\phi_i^{\mathrm{KS}}\rangle \tag{6}$$

The above constitutes a fixed-point problem due to the explicit evaluation of the self-energy at $\varepsilon_i^{\mathrm{QP}}$, and the solutions to eq 6 can be obtained iteratively or graphically on a grid with subsequent bisection refinement. As mentioned in the Introduction, if and how the obtained quasiparticle energies are used to update the self-energy via G and W defines the G_0W_0, G_nW_n, and evGW variants, respectively.

The treatment of excited states in which the number of electrons is conserved but their configuration is changed to S ($|N,0\rangle \rightarrow |N,S\rangle$) formally relies on the two-particle Green's function.[7] It is obtained as solution to the Bethe−Salpeter equation,[23] which yields the four-point density response function of the interacting system from the noninteracting system.[9,10,27]

For optical excitations, one can express coupled electron−hole amplitudes in a product basis of QP wave functions, i.e.

$$\chi_S(\mathbf{r}_e, \mathbf{r}_h) = \sum_v^{\mathrm{occ}}\sum_c^{\mathrm{unocc}}\sum_{\sigma\sigma'} A_{vc,\sigma\sigma'}^S \phi_{c,\sigma'}(\mathbf{r}_e)\phi_{v,\sigma}^*(\mathbf{r}_h)$$
$$+ B_{vc,\sigma\sigma'}^S \phi_{v,\sigma'}(\mathbf{r}_e)\phi_{c,\sigma}^*(\mathbf{r}_h) \tag{7}$$

where $\mathbf{r}_e$ ($\mathbf{r}_h$) is for the electron (hole) coordinate, and we drop the label QP for clarity. Here, $A_{vc,\sigma\sigma'}$ ($B_{vc,\sigma\sigma'}$) are the expansion coefficients of the excited-state wave function in terms of resonant (antiresonant) transitions between QP occupied

(occ.) states v and unoccupied (unocc.) c with spin σ and σ', respectively.

This basis transforms the BSE into an effective two-particle Hamiltonian problem of the form

$$
\begin{pmatrix} \underline{H}^{\text{res}} & \underline{K} \\ -\underline{K} & -\underline{H}^{\text{res}} \end{pmatrix} \begin{pmatrix} A^S \\ B^S \end{pmatrix} = \Omega_S \begin{pmatrix} A^S \\ B^S \end{pmatrix}
\tag{8}
$$

When spin−orbit coupling is negligible, this Hamiltonian has a block structure in terms of the spin combinations[36] and can be decomposed into independent Hamiltonians for singlet and triplet excitations, respectively. Dropping, therefore, the explicit spin variables, the matrix elements of $\underline{H}^{\text{res}}$ and $\underline{K}$ are calculated as

$$
H^{\text{res}}_{vc,v'c'} = D_{vc,v'c'} + \kappa K^{\text{x}}_{vc,v'c'} + K^{\text{d}}_{vc,v'c'}
\tag{9}
$$

$$
K_{cv,v'c'} = \kappa K^{\text{x}}_{cv,v'c'} + K^{\text{d}}_{cv,v'c'}
\tag{10}
$$

where $\kappa = 2$ (0) for spin singlet (triplet) excitations, and

$$
D_{vc,v'c'} = (\varepsilon_c - \varepsilon_v)\delta_{vv'}\delta_{cc'},
\tag{11}
$$

$$
K^{\text{x}}_{vc,v'c'} = \int d^3 r_e d^3 r_h \phi_c^*(r_e)\phi_v(r_e)v_c(r_e, r_h)
$$
$$
\times \phi_{c'}(r_h)\phi_{v'}^*(r_h)
\tag{12}
$$

$$
K^{\text{d}}_{vc,v'c'} = -\int d^3 r_e d^3 r_h \phi_c^*(r_e)\phi_{c'}(r_e)W(r_e, r_h, \omega = 0)
$$
$$
\times \phi_v(r_h)\phi_{v'}^*(r_h).
\tag{13}
$$

The term D represents a free interlevel transition between occupied and empty quasiparticle states; the *direct interaction* K^{d} is responsible for the binding of the electron−hole pair and is based on the attractive, but screened, interaction W (in the static approximation $\omega = 0$) between electron and hole. The repulsive *exchange interaction* K^{x} is responsible for the singlet−triplet splitting.

In systems for which the elements of the off-diagonal blocks $\underline{K}$ in eq 8 are negligible, it is legitimate to use the Tamm−Dancoff approximation (TDA),[37] in which the electron−hole amplitude is expressed as

$$
\chi_S^{\text{TDA}}(r_e, r_h) = \sum_v^{\text{occ}} \sum_c^{\text{unocc}} A^S_{\text{TDA},vc}\phi_c(r_e)\phi_v^*(r_h)
\tag{14}
$$

i.e., by resonant transitions from occupied v to unoccupied c states only. The effective Hamiltonian reduces to the upper diagonal block of eq 8

$$
\underline{H}^{\text{res}} A^S_{\text{TDA}} = \Omega_S^{\text{TDA}} A^S_{\text{TDA}}
\tag{15}
$$

2.2. Implementation Using Gaussian-Type orbitals.
The DFT and GW-BSE steps outlined above are performed with the VOTCA-XTP package.[27,38] It uses Gaussian-type orbitals $\varphi_\alpha(r)$ to expand the one- and two-point quantities. Of particular importance is the evaluation of the 4-center Coulomb repulsion integrals

$$
(\alpha\beta|\alpha'\beta') = \iint d^3 r d^3 r' \frac{\varphi_\alpha(r)\varphi_\beta(r)\varphi_{\alpha'}(r')\varphi_{\beta'}(r')}{|r - r'|}
\tag{16}
$$

which are approximated using a resolution-of-identity (RI) technique as

$$
(\alpha\beta|\alpha'\beta') \approx \sum_{\mu,\nu} (\alpha\beta|\mu)(\mu|\nu)^{-1}(\nu|\alpha'\beta')
\tag{17}
$$

where $(\mu|\nu)^{-1}$ is an element of the inverse of the 2-center repulsion matrix

$$
(\mu|\nu) = \iint d^3 r d^3 r' \xi_\mu(r)\frac{1}{|r - r'|}\xi_\nu(r')
\tag{18}
$$

and $(\alpha\beta|\mu)$ is an element of the 3-center repulsion tensor

$$
(\alpha\beta|\mu) = \iint d^3 r d^3 r' \varphi_\alpha(r)\varphi_\beta(r)\frac{1}{|r - r'|}\xi_\mu(r')
\tag{19}
$$

Within the RI approximation, the matrix elements of the self-energy operator

$$
\Sigma_{mn}(E) = \langle \phi_m^{\text{KS}}|\hat{\Sigma}(E)|\phi_n^{\text{KS}}\rangle
$$

as needed in the QP Hamiltonian read

$$
\Sigma_{mn}(E) = \sum_{\mu,\nu} \sum_l I_\mu^{ml} I_\nu^{nl} \frac{i}{2\pi} \int d\omega \frac{e^{i\omega\theta}\epsilon_{\mu\nu}^{-1}(\omega)}{E + \omega - \varepsilon_l \pm i\eta}
\tag{20}
$$

where the factor with $\theta \to 0^+$ ensures convergence of the integral, and the imaginary perturbations $\pm i\eta$ avoid singularities on the real axis, where the plus (minus) is taken when l is occupied (unoccupied). Further

$$
I_\mu^{ml} = \sum_\nu (\mu|\nu)^{-1/2} \sum_{\alpha,\beta} c_\alpha^m c_\beta^l (\alpha\beta|\nu) = \sum_\nu (\mu|\nu)^{-1/2} M_\nu^{ml}
\tag{21}
$$

and

$$
\epsilon_{\mu\nu}(\omega) = \delta_{\mu\nu} - 2 \sum_m^{\text{occ}} \sum_l^{\text{unocc}} I_\mu^{ml} I_\nu^{ml} \left[\frac{1}{\omega - (\varepsilon_m - \varepsilon_l) + 2i\eta} - \frac{1}{\omega + (\varepsilon_m - \varepsilon_l) - 2i\eta} \right]
\tag{22}
$$

is the dielectric matrix.

2.3. Models for the Self-Energy.
To evaluate the frequency integration in eq 20, we separate the self-energy $\Sigma = iGW$ into its bare exchange part $\Sigma_x = iGv_c$ and its correlation part $\Sigma_c = iG\tilde{W}$, where $\tilde{W} = W - v_c$. We briefly summarize two methods for the treatment of the correlation part in the following. For the sake of a compact presentation, the reader is referred to refs 22 and 38 for the full technical details.

The fully analytical approach (FAA) yields an exact expression and requires the calculation of the reducible polarizability $\hat{P}$. We can express it in terms of an eigenvalue decomposition of the RPA Hamiltonian (with $\kappa = -1$ and $K^{\text{d}} = 0$ in eqs 9 and 10). Eventually, the matrix entries of the correlation part of the self-energy are given by

$$
\Sigma_{c,mn}^{\text{FAA}}(E) = 2 \sum_{l,S} \frac{R_{ml}^S R_{nl}^S}{E - \varepsilon_l \pm (\Omega_S^{\text{RPA}} - i\eta)}
\tag{23}
$$

where $\pm$ denotes $+$ $(-)$ for l occupied (unoccupied), and the factor 2 accounts for spin degeneracy. The residues R_{mn}^S are calculated as

$$
R_{mn}^S = \sum_{\mu,\nu} \sum_v^{\text{occ}} \sum_c^{\text{unocc}} I_\mu^{mn} I_\nu^{vc} (A_{vc}^{S,\text{RPA}} + B_{vc}^{S,\text{RPA}})
\tag{24}
$$

Due to the high computational cost involved in diagonalizing the RPA Hamiltonian, the application of the FAA to large systems is typically not feasible.[10] Instead, the frequency dependence of the self-energy can be approximated using a generalized plasmon-pole model (PPM).[39,40] It is based on the expression of the dielectric matrix in terms of its eigenvalues $\lambda_{\mu'}$ and eigenvectors $\Phi_{\mu'}$ as

$$\epsilon_{\mu\nu}(\omega) = \sum_{\mu'} \Phi_{\mu'}^{\mu}(\omega)\lambda_{\mu'}(\omega)\Phi_{\mu'}^{\nu}(\omega) \tag{25}$$

Specifically, it is assumed in the PPM that only the eigenvalues $\lambda_{\mu'}$ depend approximately on ω

$$\lambda_{\mu'}^{-1}(\omega) \approx 1 + \frac{z_{\mu'}\omega_{\mu'}}{2}\left[\frac{1}{\omega - (\omega_{\mu'} - i\eta)} - \frac{1}{\omega + (\omega_{\mu'} - i\eta)}\right] \tag{26}$$

while eigenvectors are frequency independent. Here, $z_{\mu'}$ denotes the plasmon-pole weight, and $\omega_{\mu'}$ denotes the plasmon-pole frequency. These two model parameters are found by fitting the plasmon-pole model to the exact dielectric function,[41] as shown in eq 22, for the frequencies $\omega = 0$ and $\omega = iE_0$, with E_0 an additional model parameter, typically $E_0 = 0.5$ Ha. The correlation part of the self-energy results from the second term of eq 26, and its matrix entries are obtained as

$$\Sigma_{c,mn}^{PPM}(E) = 2\sum_{l,\mu'}\frac{1}{4}\frac{z_{\mu'}\omega_{\mu'}I_{\mu'}^{ml}I_{\mu'}^{nl}}{E - \varepsilon_l \pm \omega_{\mu'}} \tag{27}$$

where $\pm$ denotes $+ (-)$ for l occupied (unoccupied), and the factor 2 accounts for spin.

2.4. Computational Details. In the following, if not explicitly stated otherwise, all calculations have been performed using the cc-pVTZ basis set[42] with the optimized RI-basis from ref 43 and the hybrid PBE0 functional[28] on the DFT level. All molecular orbitals are used for the calculation of the screening in the RPA step of GW and in the product basis of the electron–hole wave functions in the BSE. For G_0W_0 and $G_{50}W_{50}$, we determine the quasiparticle corrections to all molecular orbital energies. However, while in evGW, only the lowest $2n_{occ}$ (all n_{occ} doubly occupied and the lowest n_{occ} unoccupied orbitals) are explicitly corrected, and the higher levels are scissors shifted according to the highest absolute quasiparticle correction among the explicitly corrected unoccupied orbitals.

The Z-matrix coordinates of a molecule are used for GW-BSE geometry optimizations. The geometry is updated according to numerical gradients of the excited-state energy with respect to internal coordinates using the Broyden–Fletcher–Goldfarb–Shanno method. The numerical gradients are evaluated by computing the central difference with displacements of $10^{-3} a_B$ in the bond lengths and 10^{-2} deg in the bond and dihedral angles. The algorithm begins at the optimized DFT ground-state geometry and proceeds iteratively until the forces are smaller than 10^{-3} Hartree/Bohr and 10^{-4} Hartree/deg for the bond lengths and (bond and dihedral) angles, respectively.

3. RESULTS

3.1. Carbon Monoxide. As described in Section 2, GW-BSE calculations can be performed in different forms depending on the treatment of the frequency dependence of the self-energy (FAA vs PPM), the level of self-consistency (G_0W_0 vs G_nW_n vs evGW), both related to the GW step, and the use of the full BSE (eq 8) vs the TDA (eq 15). To illustrate the effects of the

different approximations on the obtained excited-state total energies and optimized geometries, we consider in this section the one-dimensional potential energy surface of the excited-state $A^1\Pi$ in carbon monoxide as a function of carbon–oxygen distance (d_{C-O}). All 60 molecular orbitals are included in the RPA calculation and in the determination of quasiparticle energies in G_0W_0 and $G_{50}W_{50}$, respectively. For evGW, explicit corrections are computed for the lowest 14 molecular orbitals. In all cases, the BSE product space is formed with 7 occupied and 53 unoccupied orbitals.

Figure 1(a) shows the influence of the different levels at the GW step. Results obtained with the FAA (PPM) are shown as
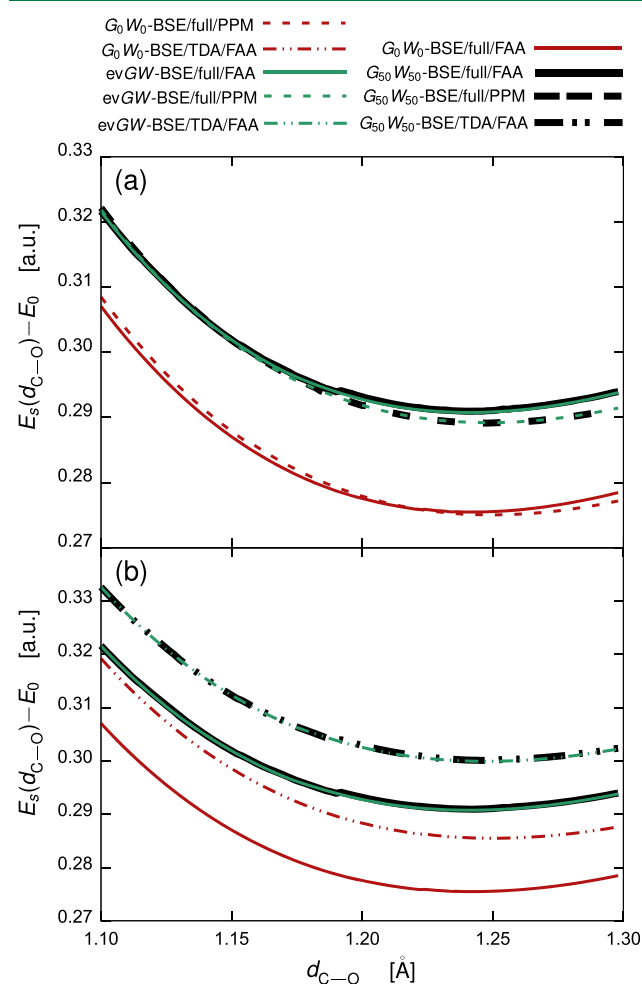

Figure 1. Total energy of the $A^1\Pi$ excited state in CO as a function of bond length d_{C-O}, relative to the energy of the optimized ground state E_0. (a) Results for the full BSE with G_0W_0-BSE (red), $G_{50}W_{50}$-BSE (black), and evGW-BSE (green) variants using the cc-pVTZ basis and the PBE0 hybrid functional in the underlying DFT calculation, employing both the FAA (full lines) and PPM (dashed lines) for the frequency dependence of the self-energy. (b) Results for the G_0W_0-BSE (red), $G_{50}W_{50}$-BSE (green), and evGW-BSE (blue) variants with the FAA using the full BSE (full lines) and TDA (dashed lines).

solid (dashed) lines, while G_0W_0 is indicated by red, $G_{50}W_{50}$ by green, and evGW by blue. Considering the FAA, as expected, the G_0W_0 curve is obtained as about 0.12 Hartree lower in energy than with the iterative approaches, mainly due to the too small quasiparticle gap in the one-shot version. Both $G_{50}W_{50}$ and evGW show unsurprisingly very similar results. However, at a distance of 1.19 Å, the $G_{50}W_{50}$ curve exhibits a faint step. This is

due to the fact that when all molecule orbital energies are quasiparticle-corrected, states with high energy are characterized by a highly structured frequency dependence of the self-energy. As a consequence, finding solutions to the quasiparticle equation (eq 6) at the required accuracy is numerically difficult and even more so due to the existence of multiple possible solutions over a small energy interval. This problem is avoided in the evGW calculation by restricting the number of explicitly quasiparticle-corrected orbitals, as mentioned above.

Employing the PPM (dashed lines in Figure 1) yields excited-state PESs with little difference to their FAA counterparts, and the same observations regarding the difference of G_0W_0 to the iterative methods can be made as in the FAA case. However, there is no visually discernible difference between the $G_{50}W_{50}$ and evGW results, which can be attributed to the less structured self-energy in the PPM. In Figure 1(b), we compare the same $A^1\Pi$ excited-state PES obtained when using the TDA instead of the full BSE on top of the different GW versions with the FAA. Generally, the TDA energies are roughly 0.1 Hartree higher, although the curvature of the PESs are very similar.

Finally, we summarize in Table 1 the optimal carbon−oxygen bond length obtained by the various methods, compared to the

Table 1. Optimized Bond Length (Å) in the $A^1\Pi$ Excited State of Carbon Monoxide, As Obtained from Different GW-BSE Variants with the cc-pVTZ Basis and PBE0 Hybrid Functional in the Underlying DFT Calculation

	full BSE		TDA	
	FAA	PPM	FAA	PPM
G_0W_0-BSE	1.241	1.249	1.249	1.256
$G_{50}W_{50}$-BSE	1.242	1.248	1.247	1.256
evGW-BSE	1.241	1.248	1.248	1.255
G_0W_0-BSE[a]				1.26
CIS[b]	1.213			
CIS(D)[b]	1.263			
EOM-CCSD[b]	1.224			
Exp.[c]	1.235			

[a]From ref 25, plane wave basis. [b]From ref 44, pVTZ+ basis. [c]From ref 45.

literature. In all cases, we can see that the different GW-BSE methods hardly influence the location of the minimum (no deviation larger than 0.002 Å). The use of the PPM leads to a slightly enlarged bond (up to 0.008 Å for the full BSE and 0.009 Å for the TDA). Similarly, using the TDA for the same self-energy method also leads to bond lengths being less than 0.01 Å shorter than for the full BSE. Our G_0W_0-BSE/TDA/PPM result (1.256 Å) is also in agreement with the value of 1.26 Å reported from a calculation with a plane wave basis.[25] The optimized bond length of the formally most precise method with the fewest approximations, evGW-BSE/full/FAA, of 1.241 Å is close to the experimentally determined value of 1.235 Å.

The above results for CO were obtained by finely scanning the excited-state total energy as a function of its bond length. For molecules with more degrees of freedom, such a procedure is impractical, and instead energy-gradient-based optimization algorithms need to be employed. Due to the lack of analytic expression for the gradients of the respective GW-BSE methods, numerical differentiation has to be used. The steps observed in the total energies of CO with the $G_{50}W_{50}$ method clearly indicates that this variant is unsuitable for yielding an accurate gradient. In the following, we therefore focus on the evaluation of G_0W_0- and evGW-based BSE approaches for the geometry optimization of a set of small molecules in excited states.

3.2. Acetone. We start with the optimization of the $n \rightarrow \pi^*$ excited state of acetone ($1^1A''$) with C_s symmetry imposed. This structure is due to the pyramidalization of the central carbon atom out of the molecular plane, and it allows one to address the quality of predictions of bond lengths, bond angles, and dihedrals in a single small molecule. All 204 molecular orbitals are included in the RPA calculation and in the determination of quasiparticle energies in G_0W_0. For evGW, explicit corrections are computed for the lowest 32 molecular orbitals, while the BSE product space is formed with 16 occupied and 172 unoccupied orbitals. The resulting optimized structural parameters are listed in Table 2, together with reference data from the literature. Deviations from the respective results obtained with CASPT2 are given in parentheses. Note that we chose CASPT2 as a reference for the analysis since it has been shown to compare

Table 2. Optimized Bond Lengths (Å), Angles, and Dihedrals (deg) of the $n \rightarrow \pi^*$ Excited State ($1^1A''$) of Acetone in C_s Symmetry[a]

	C=O		C−C		θ(C−C−C)		Θ(H−C−C=O)	
G_0W_0-BSE/full/FAA	1.327	(−0.023)	1.495	(−0.001)	113.63	(+0.88)	49.83	(−2.42)
evGW-BSE/full/FAA	1.302	(−0.048)	1.504	(+0.008)	114.58	(+1.83)	50.09	(−2.16)
G_0W_0-BSE/TDA/FAA	1.321	(−0.029)	1.492	(−0.004)	114.16	(+1.41)	49.99	(−2.26)
evGW-BSE/TDA/FAA	1.303	(−0.047)	1.502	(+0.006)	114.61	(+1.86)	49.68	(−2.67)
G_0W_0/full/PPM	1.327	(−0.023)	1.494	(−0.002)	113.87	(+1.12)	49.75	(−2.50)
evGW-BSE/full/PPM	1.308	(−0.042)	1.497	(+0.001)	114.27	(+1.52)	49.65	(−2.60)
G_0W_0-BSE/TDA/PPM	1.321	(−0.029)	1.490	(−0.006)	114.44	(+1.69)	49.04	(−3.21)
evGW-BSE/TDA/PPM	1.308	(−0.042)	1.496	(+0.000)	114.43	(+1.68)	49.33	(−2.92)
CASPT2[b]	1.350		1.496		112.75		52.25	
CC2[b]	1.404	(+0.054)	1.477	(−0.019)	112.63	(−0.12)	55.37	(+3.12)
VMC[b,c]	1.344	(−0.006)	1.489	(−0.007)	112.52	(−0.23)	52.16	(−0.09)
TDDFT/PBE0[b]	1.301	(−0.049)	1.493	(−0.003)	114.91	(+2.16)	51.50	(−0.75)
TDDFT/CAM-B3LYP[b]	1.295	(−0.055)	1.504	(+0.008)	114.84	(+2.09)	51.38	(−0.87)
TDDFT/M06-2X[b]	1.288	(−0.062)	1.516	(+0.020)	114.90	(+2.15)	50.10	(−2.15)

[a]Results from the different GW-BSE variants are obtained with the cc-pVTZ basis and the PBE0 hybrid functional in the underlying DFT calculation. Deviations Δ_i with respect to the CASPT2 reference are given in parentheses. [b]From ref 46. [c]With pseudopotentials and a pVDZ type basis of H and pVTZ type basis for C and O.
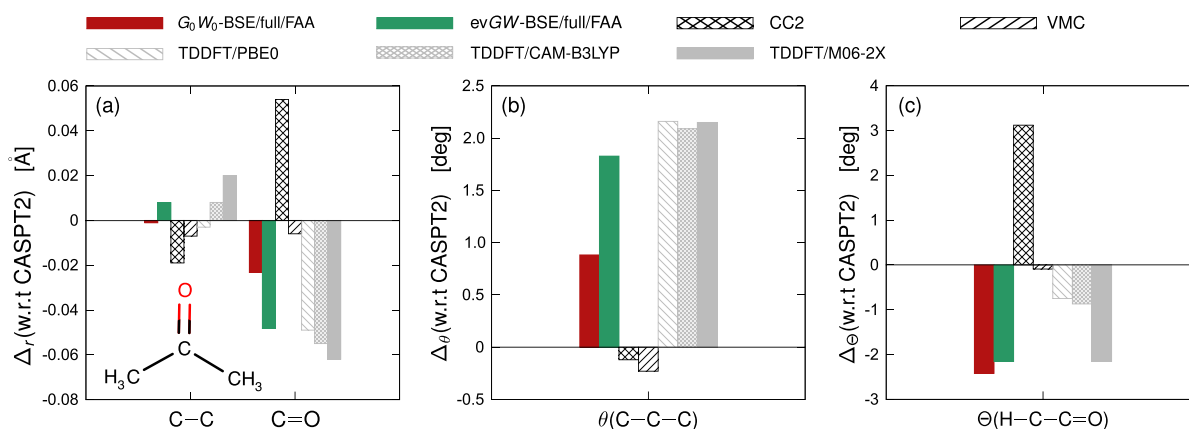
Figure 2. Deviations with respect to the CASPT2 reference of bond lengths (Å), angle, and dihedral (deg) of acetone in bent C_s symmetry resulting from G_0W_0-BSE/full/FAA (red) and evGW-BSE/full/FAA (green) optimizations of the $n \rightarrow \pi^*$ excited state, as well as CC2, VMC, and TDDFT results.
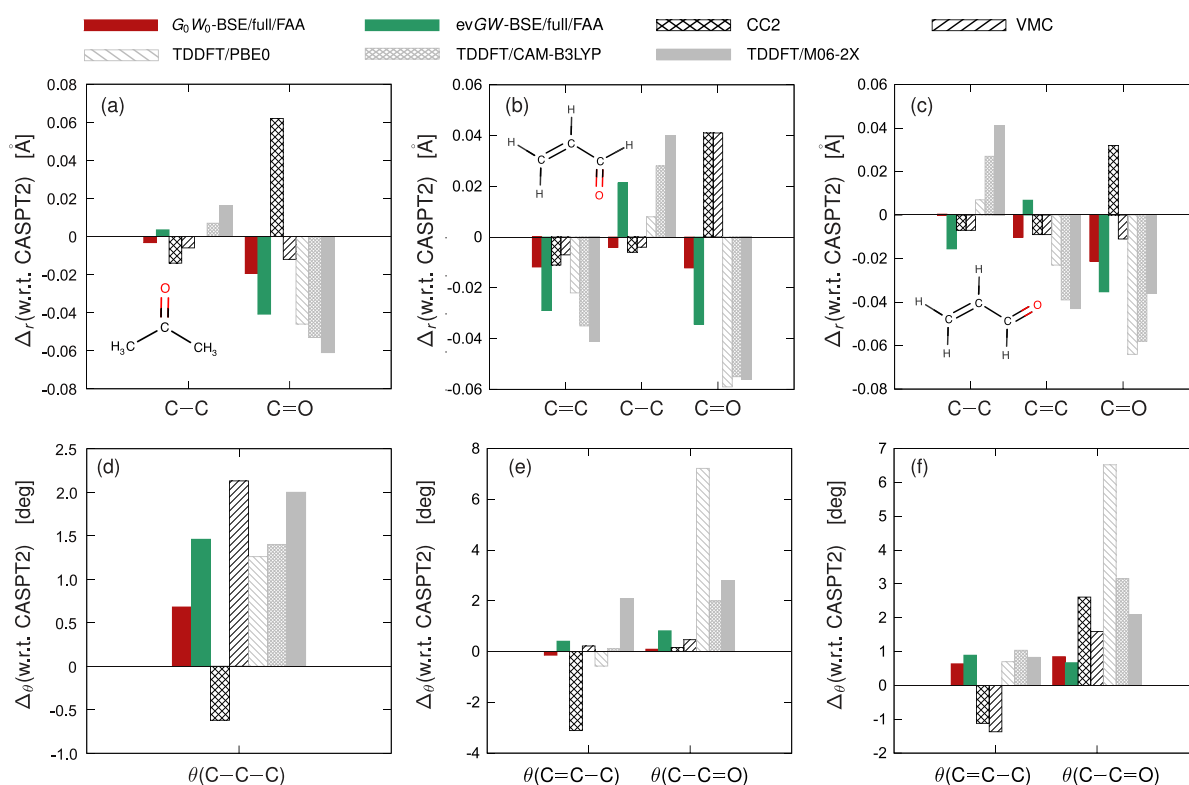

Figure 3. Deviations with respect to CASPT2 reference of bond lengths (Å) and angles (deg) of acetone in planar C_{2v} symmetry (a, d), s-cis (b, e), and s-trans acrolein (c, f) as resulting from G_0W_0-BSE/full/FAA (red) and evGW-BSE/full/FAA (green) $n \rightarrow \pi^*$ excited-state optimizations, as well as CC2, VMC, and TDDFT results. See insets for atom definitions.

favorably with CC3[47] and since it has previously been used in a similar study,[46] which makes the data readily available.

Across the eight different GW-BSE variants, the obtained C=O (C−C) bond lengths agree within 0.048 Å (0.008 Å) or better with the CASPT2 reference. The quality of the predictions is slightly better than that of TDDFT or CC2 but overall a bit worse than VMC. Similar observations can be made for the C−C−C angle, where the GW-BSE optimizations yield values between 0.88° and 1.86° larger than CASPT2. For comparison, the deviations of the TDDFT results from this reference are around 2.1°, while it is −0.12° for CC2 and −0.23° in VMC. All GW-BSE variants consistently underestimate the H−C−C=O dihedral angle in a range from 2.16° to 3.21°. Interestingly, this is

very similar to what is obtained for TDDFT/M06-2X but larger than TDDFT with PBE0 and CAM-B3LYP functionals.

From the data in Table 2, it is apparent that while there is some variation in the results of the GW-BSE methods, it is mostly similar in variation to the variations of TDDFT depending on the choice of the functional. We focus therefore in the following on the two approaches with the least approximations: G_0W_0-BSE/full/FAA (red) and evGW-BSE/full/FAA (green) as visualized in Figure 2. It is interesting to note that the one-shot approach yields better bond lengths and angles than the version with eigenvalue self-consistency, while for the dihedral both are comparable. This is in contrast to what is known for the excitation energies from the ground-state

Table 3. Optimized Bond Lengths (Å), Angles, and Dihedrals (deg) of the $n \rightarrow \pi^*$ Excited State ($1^1A''$) of Acetone in C_s Symmetry[a]

	C=O		C−C		θ(C−C−C)		Θ(H−C−C=O)	
G_0W_0-BSE/full/FAA@PBE0	1.327	(−0.023)	1.495	(−0.001)	113.63	(+0.88)	49.83	(−2.42)
G_0W_0-BSE/full/FAA@PBE	1.380	(+0.030)	1.481	(−0.015)	112.97	(+0.22)	49.31	(−2.94)
G_0W_0-BSE/full/FAA@RPA	1.335	(−0.015)	1.496	(+0.000)	113.33	(+0.58)	50.25	(−2.00)
evGW-BSE/full/FAA@PBE0	1.302	(−0.048)	1.504	(+0.008)	114.58	(+1.83)	50.09	(−2.16)
evGW-BSE/full/FAA@PBE	1.321	(−0.029)	1.515	(+0.019)	114.27	(+1.52)	50.09	(−2.16)
evGW-BSE/full/FAA@RPA	1.309	(−0.041)	1.506	(+0.010)	113.93	(+1.18)	50.03	(−2.22)

[a]Results from G_0W_0-BSE/full/FAA and evGW-BSE/full/FAA are obtained with the cc-pVTZ basis for different evaluations of the ground-state energy (PBE0, PBE, RPA) in the underlying DFT calculation. Deviations Δ_i with respect to the CASPT2 reference are given in parentheses.

structure, where evGW is generally considered to be superior to G_0W_0.

When imposing C_{2v} symmetry, the structure of acetone in its $n \rightarrow \pi^*$ excited state is planar. On the basis of the findings on the bent C_s geometry, we restrict the explicit discussion of GW-BSE-optimized geometries to those obtained with G_0W_0-BSE/full/FAA and evGW-BSE/full/FAA and compare them to reference methods. Structural parameters for all GW-BSE variants are summarized in Table S2 in the Supporting Information (SI). Figure 3(a) shows the deviations of the optimized carbon−carbon bond length with respect to the CASPT2 results. Overall, we notice a behavior consistent with that of the C_s structure (Figure 2). In both G_0W_0-BSE/full/FAA and evGW-BSE/full/FAA, the C−C bond lengths of 1.484 and 1.490 Å, respectively, are in very close agreement with the reference of 1.487 Å. Deviations for the C=O bond are slightly larger with the G_0W_0-BSE/full/FAA underestimating the reference value by 0.019 Å and evGW-BSE/full/FAA by 0.041 Å. Notably, these bond length deviations are slightly larger than in VMC but smaller than what is found for CC2 and TDDFT with various functionals. The same observation holds for the C−C−C angle as shown in Figure 3(d), which is overestimated in both G_0W_0-BSE/full/FAA (by 0.68°) and evGW-BSE/full/FAA (by 1.46°). Especially, the former deviation is smaller than those of TDDFT and in absolute value close to VMC.

3.2.1. Influence of the Ground-State Gradient. As mentioned in the Introduction, the excited-state GW-BSE gradient with respect to the nuclear coordinates, $\partial_R E_S$, is composed of the standard gradient of the ground-state energy $\partial_R E_0$ and the gradient of the excitation energy $\partial_R \Omega_S$. The previous section focused on the influence of different methods to obtain Ω_S for the numerical derivative when the ground state is evaluated with DFT and the PBE0 functional. The choice of this specific functional is motivated by the fact that it has been shown to be very reliable for the calculation of vertical excitation energies within GW-BSE.[21,27]

In order to scrutinize the influence of the ground-state gradient, we here first repeat the optimization of the excited state of acetone in C_s symmetry with the PBE functional and restrict ourselves to the G_0W_0-BSE/full/FAA and evGW-BSE/full/FAA versions. The respective results are given in Table 3. As a general observation, PBE is known to overestimate bond lengths in the ground state, while the hybrid PBE0 underestimates them, and we can see a similar trend in the optimized excited-state geometries. For instance, the C=O bond is elongated by 0.053 Å in G_0W_0-BSE/full/FAA compared to the PBE0 result and by 0.019 Å in evGW-BSE/full/FAA. We observe small variations also for bond and dihedrals angles.

As an alternative, we also consider different evaluation of the ground-state energy. On the basis of the DFT orbitals, the total

energy is not determined using the DFT exchange-correlation functional but the full Hartree−Fock-like exchange and RPA correlation energy, i.e., $E_0 = E_0^{DFT} - E_{xc} + E_x + E_c^{RPA}$. Specifically, the correlation is given as[48]

$$E_c^{RPA} = \frac{1}{2}\text{tr}(\underline{M}^{1/2} - \underline{H}^{RPA,res}) \tag{28}$$

where $\underline{M} = (\underline{H}^{RPA,res} - \underline{K}^{RPA})^{1/2}(\underline{H}^{RPA,res} + \underline{K}^{RPA})(\underline{H}^{RPA,res} - \underline{K}^{RPA})^{1/2}$ and $\underline{H}^{RPA,res}$ ($\underline{K}^{RPA}$) is the resonant (antiresonant) part of the RPA Hamiltonian with $\kappa = -1$ and $K^d = 0$ in eqs 9 and 10. This approach can formally be considered the limit of a BSE ground-state energy[49,50] with an unscreened Coulomb potential. The resulting optimized excited-state structural parameters using PBE0 orbitals in E_x and E_c^{RPA} for acetone C_s are also given in Table 3. Some smaller changes are noted with respect to the calculations with the standard PBE0 ground-state energy. In G_0W_0-BSE/full/FAA (evGW-BSE/full/FAA), the C=O bond extends by 0.008 Å (0.007 Å) and the C−C bond by 0.001 Å (0.002 Å). The C−C−C angle is minimally reduced by 0.30° (0.65°) for G_0W_0-BSE/full/FAA (evGW-BSE/full/FAA), and similarly small variations are seen for the H−C−C=O dihedral.

Evidently, the specific choice of method for evaluating the ground-state energy influences the excited-state optimization to some extent. From the obtained structural parameters, no clear preference for either of the methods can be determined. In order to facilitate a systematic comparison with the literature data, in particular, with TDDFT and the various hybrid functionals, we focus on evaluating the ground-state energy with the standard DFT energy and the PBE0 functional for the remainder of this work.

3.3. Acrolein. The preceding analysis of acetone in the $n \rightarrow \pi^*$ excited state has indicated that the G_0W_0-BSE/full/FAA method provides optimized geometries closer to those of the CASPT2 reference than the evGW-BSE/full/FAA version. To scrutinize whether this notion also holds in more general cases, we now consider the same type of excitation in *s*-cis and *s*-trans configurations of acrolein and optimize the respective structures in a planar geometry. For both configurations, all 176 molecular orbitals are included in the RPA calculation and in the determination of quasiparticle energies in G_0W_0. In evGW, explicit corrections are computed for the lowest 30 molecular orbitals, while the BSE product space is formed with 15 occupied and 161 unoccupied orbitals.

Detailed structural parameters of the optimized structure for *s*-cis acrolein resulting from all GW-BSE methods are summarized in Table S3 of the Supporting Information. In Figure 3, we show the deviations of the bond lengths (panel b) and angles (panel e) with respect to the CASPT2 reference. Overall, we notice that, as in the case of acetone, the G_0W_0-BSE/full/FAA method yields structures in closer agreement with

CASPT2 than evGW-BSE/full/FAA. For instance, the C=C bond length is shorter by 0.012 Å in G_0W_0-BSE/full/FAA but shorter by 0.029 Å in evGW-BSE/full/FAA. A similar ratio between the two methods is also found for the C−C and C=O bond. In fact, the deviations seen with G_0W_0-BSE/full/FAA are very close to those obtained with CC2 and VMC, respectively. The evGW-BSE/full/FAA results for the bonds, on the other hand, are comparable to those registered for TDDFT with different functionals and on average slightly better. For the two angles in Figure 3(f), the same general observations can be made.

For s-trans acrolein (see full data in Table S4 of the Supporting Information), the deviations of the two GW-BSE methods, as well as those of CC2, VMC, and the TDDFT variants with respect to CASPT2, are shown in panels (c, bonds) and (f, angles) of Figure 3. Among the three bonds, we note the smallest deviation for the C−C bond in G_0W_0-BSE/full/FAA, while the C=C (C=O) bond is underestimated by 0.010 Å (0.019 Å) with respect to CASPT2. We note again that evGW-BSE/full/FAA results are slightly worse in comparison but overall better than TDDFT. For the two angles in Figure 3(f), a behavior similar to that of s-cis acrolein is visible; both show that GW-BSE variants yield results that are comparable to those of CC2 and VMC and in the case of the C−C=O angle significantly better than TDDFT with the various functionals.

3.4. Methylenecyclopropene. Having established in the previous sections that the excited-state geometries optimized with the G_0W_0-BSE/full/FAA and evGW-BSE/full/FAA methods provide structural parameters in good agreement with reference data for $n \rightarrow \pi^*$ transitions in a variety of small molecules, we now turn to the analysis of a $\pi \rightarrow \pi^*$ transition in methylenecyclopropene (MCP, see inset of Figure 4). In general, it is to be expected that a twist of 90° around the C=CH$_2$ group will stabilize the state with a diradical character, which is known to be problematic for for CC2 and TDDFT. To facilitate a consistent comparison, we impose planar C$_{2v}$ symmetry on the excited-state structure. In the GW-BSE calculations, all 176 molecular orbitals are included in the RPA calculation and in the determination of quasiparticle energies in G_0W_0. For evGW, explicit corrections are computed for the lowest 28 molecular orbitals, while the BSE product space is formed with 14 occupied and 162 unoccupied orbitals, respectively. The deviations of the optimized bond lengths and angles from the CASPT2 reference are shown in Figure 4 (see Table S5 in the Supporting Information for full details).

We note that we label the bonds in the following and as shown in the inset Figure 4(a) according to the double/single bond character in the ground state. In the excited state, this character is inverted for C$_1$−C$_3$ and C$_4$=C$_3$ in the GW-BSE optimizations, in agreement with the literature. In general, the bond length deviations in panel (a) reveal a satisfying agreement: for G_0W_0-BSE/full/FAA, we note that the length of the C$_1$=C$_2$ bond of 1.455 Å is very close to the prediction of CC2 and VMC and with that significantly better than TDDFT. On the other hand, the evGW-BSE/full/FAA result exhibits a deviation of −0.025 Å very similar to that of TDDFT/PBE0. Interestingly, the trend of the G_0W_0-BSE/full/FAA results being closer to the CASPT2 reference than we observed for the $n \rightarrow \pi^*$ excited states does not appear to hold for the C$_1$−C$_3$ and C$_4$=C$_3$ bonds of MCP. Instead, the deviations of the evGW-BSE/full/FAA method are significantly smaller. For C$_1$−C$_3$, it is only −0.011 Å compared to −0.020 Å and 0.007 Å compared to 0.028 Å for C$_4$=C$_3$, respectively. Also for the angles as shown in
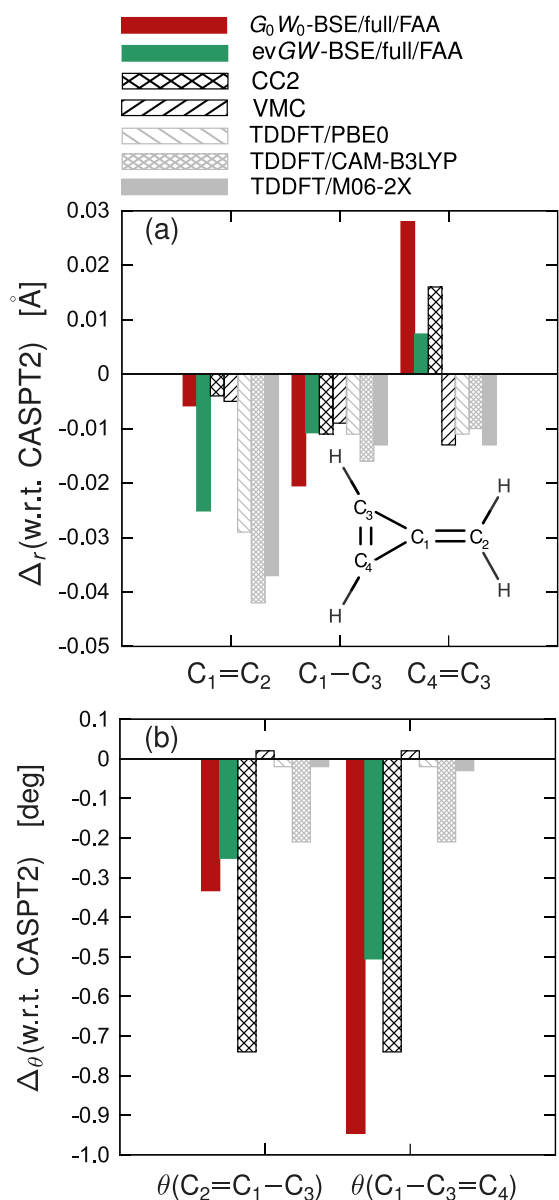

Figure 4. Deviations with respect to the CASPT2 reference of bond lengths (Å) and angles (deg) of MCP resulting from G_0W_0-BSE/full/FAA (red) and evGW-BSE/full/FAA (green) optimizations of the $\pi \rightarrow \pi^*$ excited state with C$_{2v}$ symmetry, as well as CC2, VMC, and TDDFT results.

Figure 4(b), our results indicate that the evGW-BSE/full/FAA variant yields more reliable excited-state structural properties than G_0W_0-BSE/full/FAA.

4. DISCUSSION

From the analysis of the excited-state geometry optimizations for the different molecules in Section 3, it has become clear that GW-BSE, in general, provides structural parameters in good agreement with reference data from high level methods. It has also become apparent that the G_0W_0-BSE/full/FAA variant seemed to yield better agreement with CASPT2 data than the evGW-BSE/full/FAA method, which is usually considered to be preferred for accuracy in predicting excitation energies. However, the trend is not always clear, and in particular, for $\pi \rightarrow \pi^*$ excitations, considering self-consistency in the GW quasiparticle energies seems to perform better than the one-shot

approach. Since we restricted the explicit analysis mostly to the full BSE and FAA for the frequency dependence of the self-energy and to give an overall ranking of the different methods, we calculate the mean relative error of all structural parameters with respect to CASPT2 for all the eight different GW-BSE combination we have considered.

These average relative errors are shown in Figure 5 compared to VMC, CC2, and TDDFT with three functionals. Clearly, all
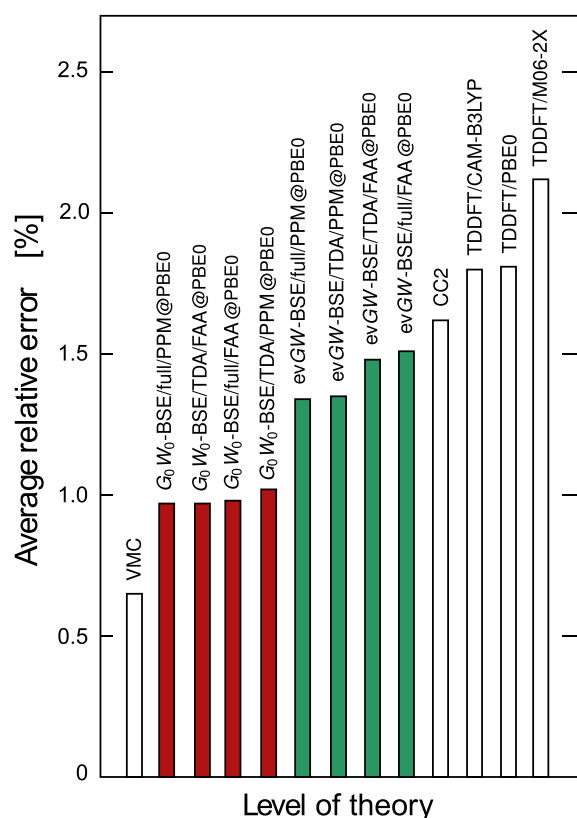

Figure 5. Methods ranked according to their average relative error (%) with respect to the CASPT2 reference.

four G_0W_0-BSE methods studied in this work exhibit an overall error around 1%, nearly independent of the approximations. In contrast, the use of the evGW-BSE methods for geometry optimization yields errors of about 1.4%–1.5%. It is interesting to note that the two variants employing the PPM are slightly better than those based in the FAA. While the smallest overall error with respect to CASPT2 is found for VMC, we also see that all GW-BSE methods perform slightly better than CC2 or TDDFT with the CAM-B3LYP, PBE0, or M06-2X functionals, respectively.

5. SUMMARY

We have presented the results of gas phase geometry optimizations in the excited states of a set of small molecules using many-body Green's functions theory within the GW approximation and the Bethe−Salpeter equation. Our results show that, overall, one-shot G_0W_0 yields geometries in slightly better agreement with the CASPT2 reference than evGW-based variants when used with a PBE0 ground state. The use of a plasmon-pole model or the Tamm−Dancoff approximation only have a negligible influence on the quality of the obtained structural parameters. We find relative errors smaller than for

CC2 and TDDFT with different functionals and only larger than VMC. Our results indicate that GW-BSE can yield geometries in good agreement with established higher-order wave function methods for small molecules.

■ ASSOCIATED CONTENT

ⓈⒾ Supporting Information

The Supporting Information is available free of charge at https://pubs.acs.org/doi/10.1021/acs.jctc.0c01099.

Full GW-BSE optimization data for acetone, acrolein, and methylenecyclopropene (PDF)

■ AUTHOR INFORMATION

Corresponding Authors

Onur Çaylak − *Department of Mathematics and Computer Science and Institute for Complex Molecular Systems, Eindhoven University of Technology, 5600MB Eindhoven, The Netherlands*; Email: o.caylak@tue.nl

Björn Baumeier − *Department of Mathematics and Computer Science and Institute for Complex Molecular Systems, Eindhoven University of Technology, 5600MB Eindhoven, The Netherlands*; ⓘ orcid.org/0000-0002-6077-0467; Email: b.baumeier@tue.nl

Complete contact information is available at:
https://pubs.acs.org/10.1021/acs.jctc.0c01099

Notes

The authors declare no competing financial interest.

■ ACKNOWLEDGMENTS

■ REFERENCES

(1) Adachi, C. Third-generation organic electroluminescence materials. *Jpn. J. Appl. Phys.* **2014**, *53*, 060101.

(2) Tang, C. W.; Vanslyke, S. A. Organic electroluminescent diodes. *Appl. Phys. Lett.* **1987**, *51*, 913−915.

(3) Halls, J. J.; Walsh, C. A.; Greenham, N. C.; Marseglia, E. A.; Friend, R. H.; Moratti, S. C.; Holmes, A. B. Efficient photodiodes from interpenetrating polymer networks. *Nature* **1995**, *376*, 498−500.

(4) Baral, S.; Phillips, M.; Yan, H.; Avenso, J.; Gundlach, L.; Baumeier, B.; Lyman, E. Ultrafast Formation of the Charge Transfer State of Prodan Reveals Unique Aspects of the Chromophore Environment. *J. Phys. Chem. B* **2020**, *124*, 2643−2651.

(5) Kancherla, R.; Muralirajan, K.; Sagadevan, A.; Rueping, M. Visible Light-Induced Excited-State Transition-Metal Catalysis. *Trends Chem.* **2019**, *1*, 510.

(6) Stein, T.; Kronik, L.; Baer, R. Reliable prediction of charge transfer excitations in molecular complexesusing time-dependent density functional theory. *J. Am. Chem. Soc.* **2009**, *131*, 2818−2820.

(7) Hedin, L.; Lundqvist, S. Effects of Electron-Electron and Electron-Phonon Interactions on the One-Electron States of Solids. *Solid State Phys.* **1970**, *23*, 1−181.

(8) Hybertsen, M. S.; Louie, S. G. First-principles theory of quasiparticles: Calculation of band gaps in semiconductors and insulators. *Phys. Rev. Lett.* **1985**, *55*, 1418−1421.

(9) Onida, G.; Reining, L.; Rubio, A. Electronic excitations: Density-functional versus many-body Green's-function approaches. *Rev. Mod. Phys.* **2002**, *74*, 601−659.

(10) Golze, D.; Dvorak, M.; Rinke, P. The GW Compendium: A Practical Guide to Theoretical Photoemission Spectroscopy. *Front. Chem.* **2019**, *7*, 7.

(11) Rohlfing, M. Excited states of molecules from Green's function perturbation techniques. *Int. J. Quantum Chem.* **2000**, *80*, 807−815.

(12) Baumeier, B.; Andrienko, D.; Ma, Y.; Rohlfing, M. Excited states of dicyanovinyl-substituted oligothiophenes from many-body Green's functions theory. *J. Chem. Theory Comput.* **2012**, *8*, 997.

(13) Baumeier, B.; Andrienko, D.; Rohlfing, M. Frenkel and charge-transfer excitations in donor-acceptor complexes from many-body green's functions theory. *J. Chem. Theory Comput.* **2012**, *8*, 2790−2795.

(14) Baumeier, B.; Rohlfing, M.; Andrienko, D. Electronic excitations in push-pull oligomers and their complexes with fullerene from many-body Green's functions theory with polarizable embedding. *J. Chem. Theory Comput.* **2014**, *10*, 3104−3110.

(15) Van Setten, M. J.; Weigend, F.; Evers, F. The GW-method for quantum chemistry applications: Theory and implementation. *J. Chem. Theory Comput.* **2013**, *9*, 232−246.

(16) Van Setten, M. J.; Caruso, F.; Sharifzadeh, S.; Ren, X.; Scheffler, M.; Liu, F.; Lischner, J.; Lin, L.; Deslippe, J. R.; Louie, S. G.; Yang, C.; Weigend, F.; Neaton, J. B.; Evers, F.; Rinke, P. GW100: Benchmarking G0W0 for Molecular Systems. *J. Chem. Theory Comput.* **2015**, *11*, 5665−5687.

(17) Varsano, D.; Coccia, E.; Pulci, O.; Conte, A. M.; Guidoni, L. Ground state structures and electronic excitations of biological chromophores at Quantum Monte Carlo/Many Body Green's Function Theory level. *Comput. Theor. Chem.* **2014**, *1040−1041*, 338−346.

(18) Golze, D.; Wilhelm, J.; van Setten, M. J.; Rinke, P. Core-Level Binding Energies from *GW*: An Efficient Full-Frequency Approach within a Localized Basis. *J. Chem. Theory Comput.* **2018**, *14*, 4856−4869.

(19) Kaplan, F.; Harding, M. E.; Seiler, C.; Weigend, F.; Evers, F.; Van Setten, M. J. quasiparticle Self-Consistent GW for Molecules. *J. Chem. Theory Comput.* **2016**, *12*, 2528−2541.

(20) Boulanger, P.; Jacquemin, D.; Duchemin, I.; Blase, X. Fast and accurate electronic excitations in cyanines with the many-body bethe-salpeter approach. *J. Chem. Theory Comput.* **2014**, *10*, 1212−1218.

(21) Jacquemin, D.; Duchemin, I.; Blase, X. Benchmarking the Bethe-Salpeter Formalism on a Standard Organic Molecular Set. *J. Chem. Theory Comput.* **2015**, *11*, 3290−3304.

(22) Bruneval, F.; Rangel, T.; Hamed, S. M.; Shao, M.; Yang, C.; Neaton, J. B. MOLGW 1: Many-body perturbation theory software for atoms, molecules, and clusters. *Comput. Phys. Commun.* **2016**, *208*, 149−161.

(23) Strinati, G. Application of the Green's functions method to the study of the optical properties of semiconductors. *Riv. Nuovo Cim.* **1988**, *11*, 1−86.

(24) Casida, M. E. *Time-Dependent Density Functional Response Theory for Molecules* **1995**, *1*, 155−192.

(25) Ismail-Beigi, S.; Louie, S. G. Excited-State Forces within a First-Principles Green's Function Formalism. *Phys. Rev. Lett.* **2003**, *90*, 4.

(26) Godby, R. W.; Schlüter, M.; Sham, L. J. Self-energy operators and exchange-correlation potentials in semiconductors. *Phys. Rev. B: Condens. Matter Mater. Phys.* **1988**, *37*, 10159−10175.

(27) Wehner, J.; Brombacher, L.; Brown, J.; Junghans, C.; ćaylak, O.; Khalak, Y.; Madhikar, P.; Tirimbò, G.; Baumeier, B. Electronic Excitations in Complex Molecular Environments: Many-Body Green's Functions Theory in VOTCA-XTP. *J. Chem. Theory Comput.* **2018**, *14*, 6253−6268.

(28) Adamo, C.; Barone, V. Toward reliable density functional methods without adjustable parameters: The PBE0 model. *J. Chem. Phys.* **1999**, *110*, 6158−6170.

(29) Guido, C. A.; Jacquemin, D.; Adamo, C.; Mennucci, B. On the TD-DFT accuracy in determining single and double bonds in excited-state structures of organic molecules. *J. Phys. Chem. A* **2010**, *114*, 13402−13410.

(30) Guido, C. A.; Knecht, S.; Kongsted, J.; Mennucci, B. Benchmarking time-dependent density functional theory for excited state geometries of organic molecules in gas-phase and in solution. *J. Chem. Theory Comput.* **2013**, *9*, 2209−2220.

(31) Page, C. S.; Olivucci, M. Ground and excited state CASPT2 geometry optimizations of small organic molecules. *J. Comput. Chem.* **2003**, *24*, 298−309.

(32) Yanai, T.; Tew, D. P.; Handy, N. C. A new hybrid exchange-correlation functional using the Coulomb-attenuating method (CAM-B3LYP). *Chem. Phys. Lett.* **2004**, *393*, 51−57.

(33) Zhao, Y.; Truhlar, D. G. The M06 suite of density functionals for main group thermochemistry, thermochemical kinetics, noncovalent interactions, excited states, and transition elements: Two new functionals and systematic testing of four M06-class functionals and 12 other functionals. *Theor. Chem. Acc.* **2008**, *120*, 215−241.

(34) Kohn, W.; Sham, L. J. Self-consistent equations including exchange and correlation effects. *Phys. Rev.* **1965**,.

(35) Aulbur, W. G.; Jönsson, L.; Wilkins, J. W. In *Solid State Phys..*; Ehrenreich, H., Spaepen, F., Eds.; Academic Press, 2000; Vol. *54*; pp 1−218.

(36) Rohlfing, M.; Louie, S. G. Electron-hole excitations and optical spectra from first principles. *Phys. Rev. B* **2000**,.

(37) Fetter, A. L.; Walecka, J. D. *Quantum Theory of Many-Particle Systems*; Courier Corporation, 2003.

(38) Tirimbo, G.; Sundaram, V.; Çaylak, O.; Scharpach, W.; Sijen, J.; Junghans, C.; Brown, J.; Ruiz, F. Z.; Renaud, N.; Wehner, J.; Baumeier, B. Excited-state electronic structure of molecules using many-body Green's functions: quasiparticles and electron-hole excitations with VOTCA-XTP. *J. Chem. Phys.* **2020**, *152*, 114103.

(39) Hybertsen, M. S.; Louie, S. G. Electron correlation in semiconductors and insulators: Band gaps and quasiparticle energies. *Phys. Rev. B: Condens. Matter Mater. Phys.* **1986**, *34*, 5390.

(40) Godby, R. W.; Needs, R. J. Metal-insulator transition in Kohn-Sham theory and quasiparticle theory. *Phys. Rev. Lett.* **1989**, *62*, 1169.

(41) Rohlfing, M.; Krüger, P.; Pollmann, J. Efficient scheme for GW quasiparticle band-structure calculations with applications to bulk Si and to the Si(001)-(2 × 1) surface. *Phys. Rev. B: Condens. Matter Mater. Phys.* **1995**, *52*, 1905−1917.

(42) Dunning, T. H. Gaussian basis sets for use in correlated molecular calculations. I. The atoms boron through neon and hydrogen. *J. Chem. Phys.* **1989**, *90*, 1007−1023.

(43) Weigend, F.; Köhn, A.; Hättig, C. Efficient use of the correlation consistent basis sets in resolution of the identity MP2 calculations. *J. Chem. Phys.* **2002**, *116*, 3175−3183.

(44) Stanton, J. F.; Gauss, J.; Ishikawa, N.; Head-Gordon, M. A comparison of single reference methods for characterizing stationary points of excited state potential energy surfaces. *J. Chem. Phys.* **1995**, *103*, 4160−4174.

(45) Huber, K. P.; Herzberg, G. *Molecular Spectra and Molecular Structure*; Springer US, 1979.

(46) Guareschi, R.; Filippi, C. Ground- and excited-state geometry optimization of small organic molecules with quantum Monte Carlo. *J. Chem. Theory Comput.* **2013**, *9*, 5513−5525.

(47) Budzák, V.; Scalmani, G.; Jacquemin, D. Accurate Excited-State Geometries: A CASPT2 and Coupled-Cluster Reference Database for Small Molecules. *J. Chem. Theory Comput.* **2017**, *13*, 6237−6252.

(48) Eshuis, H.; Yarkony, J.; Furche, F. Fast computation of molecular random phase approximation correlation energies using resolution of the identity and imaginary frequency integration. *J. Chem. Phys.* **2010**, *132*, 234114.

(49) Holzer, C.; Gui, X.; Harding, M. E.; Kresse, G.; Helgaker, T.; Klopper, W. Bethe-Salpeter correlation energies of atoms and molecules. *J. Chem. Phys.* **2018**, *149*, 144106.

(50) Loos, P.-F.; Scemama, A.; Duchemin, I.; Jacquemin, D.; Blase, X. Pros and Cons of the Bethe-Salpeter Formalism for Ground-State Energies. *J. Phys. Chem. Lett.* **2020**, *11*, 3536−3545.